Fluid and hybrid simulations of the ionization instabilities in Hall thruster

IEPC-2019-762

Presented at the 36th International Electric Propulsion Conference
University of Vienna, Austria
September 15-20, 2019

O. Chapurin* and A. Smolyakov†
University of Saskatchewan, Saskatoon, SK S7N 5E2 CANADA
G. Hagelaar‡ and J.P. Boeuf §
Université de Toulouse, CNRS, Laboratoire Plasma et Conversion d'Energie
118 route de Narbonne, F-31062 Toulouse, FRANCE
Y. Raitses ¶
Plasma Physics Laboratory, Princeton University, Princeton, New Jersey 08543, USA

Low-frequency axial oscillations in 5-50 kHz range (commonly called breathing modes) stand out as pervasive features observed in many types of Hall thrusters. A one-dimensional time-dependent full nonlinear low-frequency model that describes neutral atoms, ions, and electrons, is developed in fluid formulation and compared to the hybrid model under one of the LANDMARK benchmarking test case. Both models include neutral atoms dynamics and ionization, self-consistent electron and ion dynamics in quasineutral plasmas, electron diffusion, and electron energy evolution. Three different cases, two of which are oscillatory, are studied and compared. The reasons for differences between fluid and hybrid results were discussed and modifications of the fluid model were suggested.

Nomenclature

α	coefficient to electron wall collision frequency
β	ionization rate coefficient
β_a	coefficient to anomalous Bohm frequency
b_v	Bohm velocity factor
B	axial distribution of radial magnetic field
c_s	ion-sound velocity
e	elementary charge
E	axial electric field
ε	electron energy
J_a	atom density flux
J_T	total (electron and ion) discharge current density
I_D	total (electron and ion) discharge current
k_m	electron neutral collision rate constant
K	electron collisional energy loss coefficient
L	channel length

*Ph.D. Student, Department of Physics and Engineering Physics, alex.chapurin@usask.ca
†Professor, Department of Physics and Engineering Physics, andrei.smolyakov@usask.ca
‡Senior Scientist, CNRS, gerjan.hagelaar@gmail.com
§Senior Scientist at CNRS, jpb@laplace.univ-tlse.fr
¶Principal Research Physicist, Plasma Science and Technology Department, yraitses@pppl.gov

μ_e	electron mobility
m_e	electron mass
m_i	Xenon ion mass
$\dot{m}$	atom mass flow rate
n	plasma density (quasineutral)
n_e	electron density
n_i	ion density
n_i	atom density
ν_m	total electron momentum exchange frequency
ν_{en}	electron-neutral collision frequency
ν_{walls}	electron-wall collision frequency
ν_B	anomalous Bohm electron frequency
ν_ε	coefficient to anomalous electron energy losses
p_e	electron isotropic pressure
q_e	electron heat flux
T_e	electron temperature
U	a constant in electron anomalous energy losses coefficient
ϕ	electric potential
v_a	atom average velocity
v_i	ion average velocity
v_{ex}	electron average velocity in axial direction
W	electron anomalous energy loss coefficient
ω_{ce}	electron-cyclotron frequency
x	axial coordinate

I. Introduction

Hall thrusters is one class of plasma devices successfully used for both electric propulsion in space and satellite orbit keeping. Such thrusters are becoming an enabling technology of choice for long term missions, e.g. trips to Mars. Despite relatively long history (since 1972) of using these devices, the physics of their operation are poorly understood. In absence of predictive modeling capabilities, scaling of these devices for large (e.g., for long term missions) and for low (for microsatellites) power is very difficult, slow and expensive.

Plasmas in Hall thrusters is supported by the electron E $\times$ B drift in the closed (periodic) azimuthal direction, and the thrust is created by unmagnetized ions accelerated by the electric field in the axial direction (in the gap between two coaxial dielectric cylinders). One of the characteristics of Hall thruster is the presence of turbulence and structures (azimuthal and axial) that affect their operation. In particular, the turbulent electron transport is orders of magnitude larger than the classical collisional transport. Studies of nonlinear phenomena in these plasmas are not only of great practical importance but also addresses fundamental problems of plasma physics and plasma turbulence. Full kinetic 2D and 3D simulations mostly remain out of practical reach due to enormous computational costs. Reduced fluid plasma simulations models based on conservation laws and derived from higher dimensional kinetic formulation are less computationally expensive and in many situations can describe important physical phenomena. A good compromise can be achieved with hybrid models, where electrons are modeled with fluid equations and ions are kinetic (e.g., particle-in-cell method). Nonetheless, fluid calculations are typically much faster and can provide more flexibility. The fluid approach also allows to construct simplified models, when one can neglect some (perhaps, important) physical effects for that purpose of capturing more essential behaviour, e.g. when investigating an instability mechanism (analysis or simulations). Time-dependent simulations of low-frequency modes in axial HT were done earlier with various plasma models, fluid,[1–3] hybrid.[1,4–6] Stationary fluid 1d solutions were presented in Refs.[7–10]

In this work multi-species full fluid model is compared to the hybrid model for a Hall thruster configuration in order to investigate possible differences and show how to overcome some of them. The model and parameters of the simulations are chosen to correspond to one of the LANDMARK benchmarking cases.[11] The hybrid and fluid models describe electrons with the same set of fluid equations, but ions and neutral atoms are described kinetically in the hybrid model. While kinetic approach offers a more accurate physical description, where velocity distribution function is also evolving in time, a good agreement is shown with fluid models with some quantitative discrepancies. In some cases, we had to modify (improve) fluid description to achieve a better result. Previously, a comparison between fluid and hybrid models for the axial direction of Hall thruster configuration was presented in Ref.,[12] however this model did not include electron pressure (thus omitting effects near absorbing wall, like presheath region and ions transition through the ion-sound barrier) and detailed electron energy balance.

II. Fluid and hybrid simulations models

The model of low-frequency axial plasma dynamics in Hall thruster is considered in electrostatic and quasineutral approximation. It includes a self-consistent electric field, neutral atoms and ionization, anode recombination, electron pressure, and electron energy balance. Three species, neutrals, ions, and electrons are used in this model, with electron inertia neglected. We will describe the full fluid model and then the hybrid model, where ions and neutrals are modeled as particles (particle-in-cell method). System length of 5 cm is assumed in the axial extent of a Hall thruster, with the channel exit at the middle, where radial magnetic field has its maximum, Fig. 1. BOUT++ computational framework[13] is used for fluid simulations, and the hybrid code developed in the LAPLACE laboratory, France.[2,14,15]

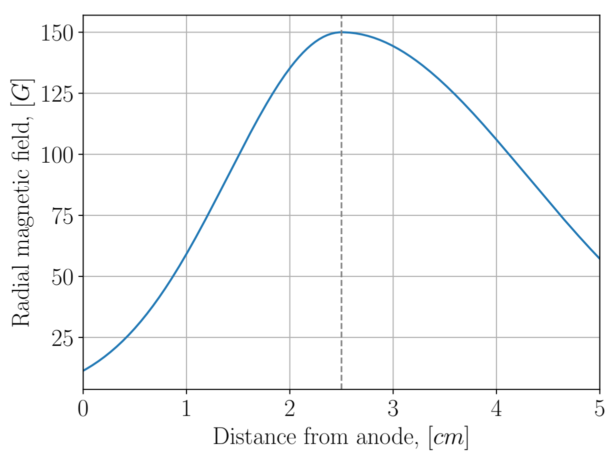

Figure 1. The magnetic field profile used in simulations, with the channel exit located 2.5 cm from anode (dashed line).

In simplest case, we assume neutral atoms flow with a constant flow velocity v_a , so that they are described with the simple advection equation

$$\frac{\partial n_a}{\partial t} + v_a \frac{\partial n_a}{\partial x} = -\beta n_a n, \tag{1}$$

where $\beta n_a n$ is the ionization source term and β is the ionization rate coefficient, obtained by BOLSIG.[16]

Ion are unmagnetized and described with basic plasma fluid equations:

$$\frac{\partial n_i}{\partial t} + \frac{\partial}{\partial x}\left(n_i v_i\right) = \beta n_a n_i, \tag{2}$$

$$\frac{\partial v_i}{\partial t} + v_i \frac{\partial v_i}{\partial x} = \frac{e}{m_i} E + \beta n_a \left(v_a - v_i\right), \tag{3}$$

where e is elementary charge, m_i is ion mass. In this form we neglect the pressure term and generalized viscosity tensor. Ion temperature evolution is also omitted due to negligible effect.

Finally, magnetized electrons are described with the following equations:

$$\frac{\partial n_e}{\partial t} + \frac{\partial}{\partial x}\left(n_e v_{ex}\right) = \beta n_n n_e, \tag{4}$$

$$0 = -\frac{e}{m_e}\mathbf{E} - \frac{eB}{m_e}\left(\mathbf{v}_{e\perp} \times \mathbf{e}_z\right) - \frac{1}{n_e m_e}\frac{\partial\left(n_e T_e\right)}{\partial x} - \nu_m \mathbf{v}_e, \tag{5}$$

$$\frac{3}{2}\frac{\partial}{\partial t}\left(nT_e\right) + \frac{5}{2}\frac{\partial}{\partial x}\left(n_e v_{ex} T_e\right) + \frac{5}{2}\frac{\partial q_e}{\partial x} = -n_e v_{ex}\frac{\partial \phi}{\partial x} - n_e n_a \mathrm{K} - n\mathrm{W}, \tag{6}$$

where m_e is electron mass, ν_m is the total electron momentum exchange frequency, W is the anomalous energy loss coefficient, K is the collisional energy loss coefficient, generated by BOLSIG,[16] and q_e is the electron heat flux. The anomalous electron energy loss coefficient W is modeled as

$$\mathrm{W} = \nu_\varepsilon \varepsilon \exp\left(-U/\varepsilon\right), \tag{7}$$

where $\varepsilon = 3/2T_e$, $U = 20\ eV$. Heat flux across magnetic field is

$$q_e = -\mu_e n T_e \frac{\partial T_e}{\partial x}. \tag{8}$$

Eq. (5) splits into two components and assuming no pressure gradients nor equilibrium electric fields in other than axial direction, the axial electron velocity is expressed:

$$v_{ex} = -\mu_e E - \frac{\mu_e}{n_e}\frac{\partial(nT_e)}{\partial x}, \tag{9}$$

where the electron mobility μ_e is known as the classical electron mobility across magnetic field:

$$\mu_e = \frac{e}{m_e \nu_m}\frac{1}{1 + \omega_{ce}^2/\nu_m^2}. \tag{10}$$

The model of electron transport as based on the assumption of the following total electron momentum exchange collision frequency:

$$\nu_m = \nu_{en} + \nu_{walls} + \nu_B, \tag{11}$$

where the electron-neutral collision frequency ν_{en}, electron-wall collision frequency ν_{walls}, and anomalous Bohm frequency ν_B are given with:

$$\nu_{en} = k_m n_a, \tag{12}$$

$$\nu_{walls} = \alpha 10^7\ [s^{-1}], \tag{13}$$

$$\nu_B = (\beta_a/16)\, eB/m_e. \tag{14}$$

where $k_m = 2.5 \times 10^{-13}\ m^{-3}s^{-1}$, α and β_a are adjusting constants.

The profile of external magnetic field is shown if Fig. 1, with the channel's exit in the peak of magnetic field intensity. For this electron mobility model we will use different parameters inside and outside the channel, the near wall conductivity contribution $\alpha_{in} = 0.2$, $\alpha_{out} = 0$. The anomalous contribution is set to $\beta_{a,in} = 0.1$, $\beta_{a,out} = 1$.

We will assume plasma quasineutrality and neglect a potential drop on the Debye sheath near the anode. The total (discharge) current density J_T is determined from the condition

$$\int_0^L E dx = U_0, \tag{15}$$

and given as

$$J_T = \frac{U_0 + \int_0^L \left(\frac{v_i}{\mu_e} + \frac{1}{n}\frac{\partial p_e}{\partial x}\right) dx}{\int_0^L \frac{dx}{en\mu_e}}. \tag{16}$$

Therefore, the full system of equations to be solved,

$$\frac{\partial n_a}{\partial t} + v_a \frac{\partial n_a}{\partial x} = -\beta n_a n, \tag{17}$$

$$\frac{\partial n}{\partial t} + \frac{\partial}{\partial x}(n v_i) = \beta n_a n, \tag{18}$$

$$\frac{\partial v_i}{\partial t} + v_i \frac{\partial v_i}{\partial x} = \frac{e}{m_i} E + \beta n_a (v_a - v_i), \tag{19}$$

$$\frac{3}{2}\frac{\partial}{\partial t}(n T_e) + \frac{5}{2}\frac{\partial}{\partial x}(n v_{ex} T_e) + \frac{5}{2}\frac{\partial q_e}{\partial x} = n v_{ex} E - n n_a \mathrm{K} - n \mathrm{W}, \tag{20}$$

where the electric field E is obtained from the electron momentum Eq. (10). This system is solved with the following boundary conditions. A constant mass flow rate determines the value of n_a at the boundary, as well as recombination of plasma that flows to the anode, hence the boundary condition:

$$N(0) = \frac{\dot{m}}{m_i A v_a} - \frac{n v_i(0)}{v_a}. \tag{21}$$

Bohm type condition for ion velocity can be imposed at the anode $v_i(0) = -b_v \sqrt{T_e/m_i}$, where $b_v = 0$–1 is the Bohm velocity factor which can be varied. Both anode and cathode electron temperature are fixed with $T_e(0) = T_e(L) = 2\ eV$. All other boundary conditions are not imposed (free).

Hybrid model has the same electron equations, while ions and neutrals are modeled via particle-in-cell method.[2,14,15] Atoms can be monoenergetic, when all particles has the same velocity (zero temperature), or thermally initialized with Maxwellian velocity distribution function.

III. Simulation results and comparison

The models described above was studied in three main test cases. In Case 1 and 2 different anomalous wall losses coefficient in Eq. (7) is used inside the thrusters channel, and neutral atoms are kept monoenergetic in the hybrid model. In Case 3 same parameters as in Case 2 are used but neutral atoms have a finite temperature, thus atoms velocity distribution function (VDF) is included. For Case 1 $\nu_{\varepsilon,\mathrm{in}} = 0.95 \cdot 10^7\ s^{-1}$, and for Case 2 $\nu_{\varepsilon,\mathrm{in}} = 0.4 \cdot 10^7\ s^{-1}$. As expected, higher electron energy losses for Case 1 results into lower average electron energy in compare to the Case 2.

Case 1 and Case 2 are both oscillatory, and Case 3 is stationary. In Case 1 along with low-frequency behaviour, we observe higher frequency ion flyby time oscillations (or transient-time oscillations),[17] they are absent in Case 2. These results are observed in both fluid and hybrid models and show only some quantitative discrepancies. It is shown, that these differences are mainly due to ion boundary condition or ion finite temperature effects. With corresponding modifications to the fluid model, these discrepancies can be reduced. In Case 3 neutral atom VDF strongly affects simulation results in the hybrid model, making it near stationary. Then the fluid model was supplemented with the atom momentum balance equation (with constant temperature) to capture this effect.

A. Case 1

As it was mentioned, this case is characterized with both low-frequency as higher frequency oscillations in the same time. This phenomena observed in both fluid and hybrid models, but the hybrid case has significantly smaller total current amplitude, Figs. 2a, 2b. Spectral power of the total current also shows the differences in both low- and high-frequency range, Figs. 2a,2b.

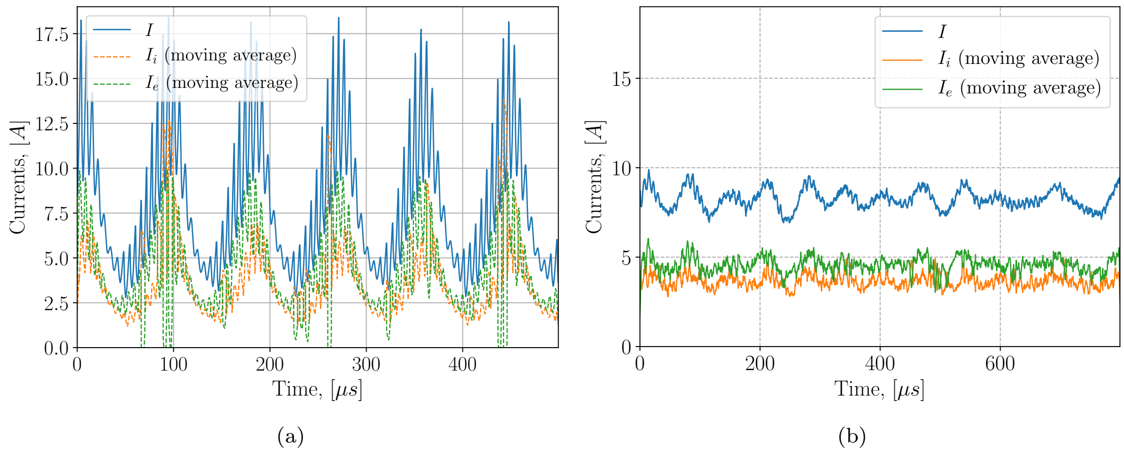

Figure 2. Total, ion, and electron current result from fluid model (a) and hybrid model (b). Ion and electron currents are evaluated at $x = 5\ cm$, Case 1.

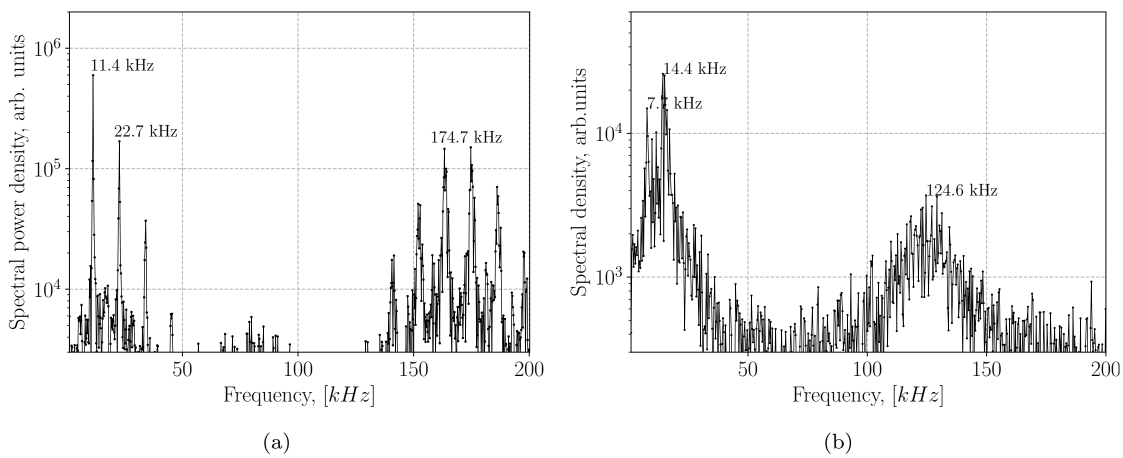

Figure 3. Spectral density of the total current for fluid model (a) and hybrid model (b), Case 1.

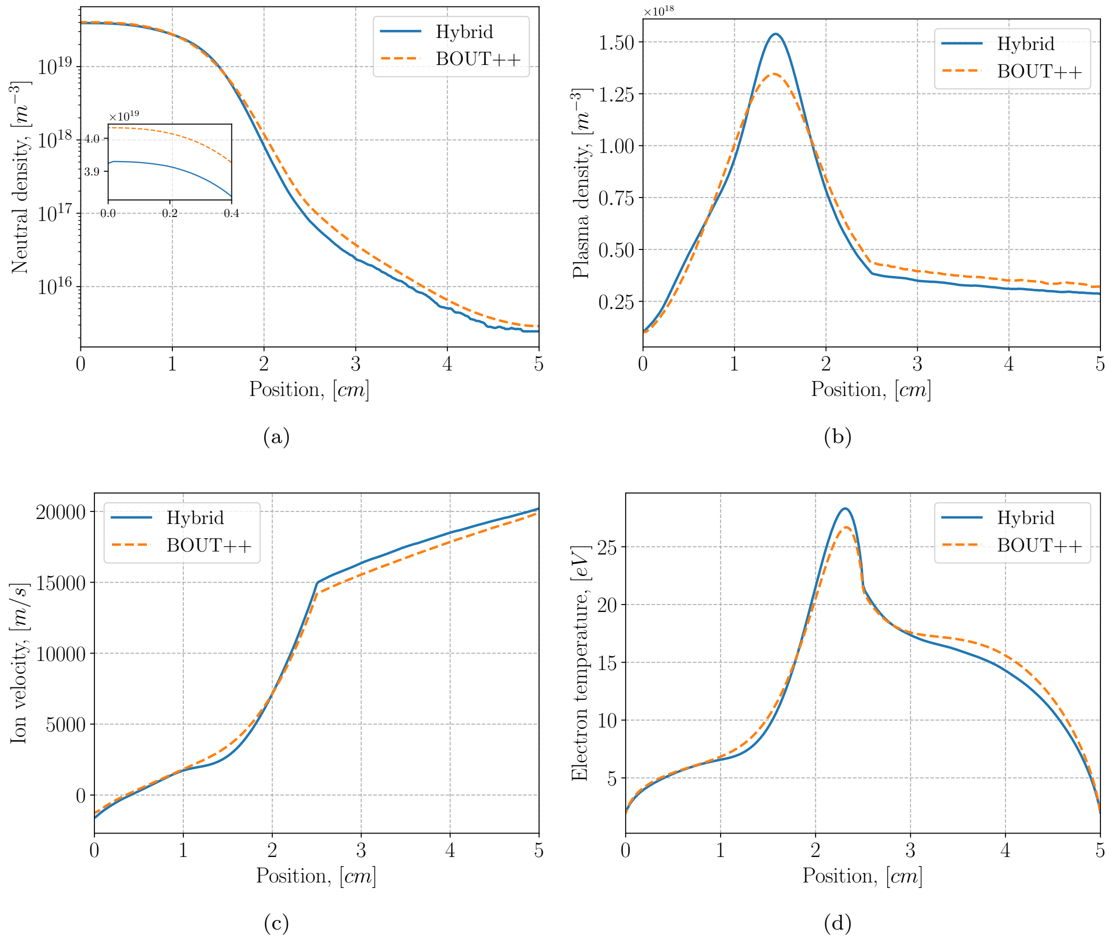

Figure 4. Comparison of spatial distribution of time averaged macroscopic profiles between fluid and hybrid models, Case 1.

It is noted that in hybrid model ion temperature might be not too low to neglect it. We have calculated the ion temperature from the kinetic part of the hybrid model as $T_i = p_{i,xx}/n_i$, where $p_{i,xx} = m_i \int v_x' v_x' f_x dv_x$, where $v_x' = v_x - V_x$ is the random particle velocity. We assumed that the ion pressure tensor is isotropic, i.e. $p_{i,xx} = p_{i,yy} = p_{i,zz}$, and cross terms are zero. Other required fluid moments were calculated from the kinetic description of ions in the hybrid model, and ion momentum balance equation is checked showing that the ion pressure term introduces notable disbalance in the ion momentum balance equation. Therefore, ion pressure term was added to the fluid model with constant $T_i = 1.2\ eV$, which made the total current amplitude and frequency closer to the hybrid model results. Averaged macroscopic plasma variables were also in a better agreement, Figs. 6a-6d.

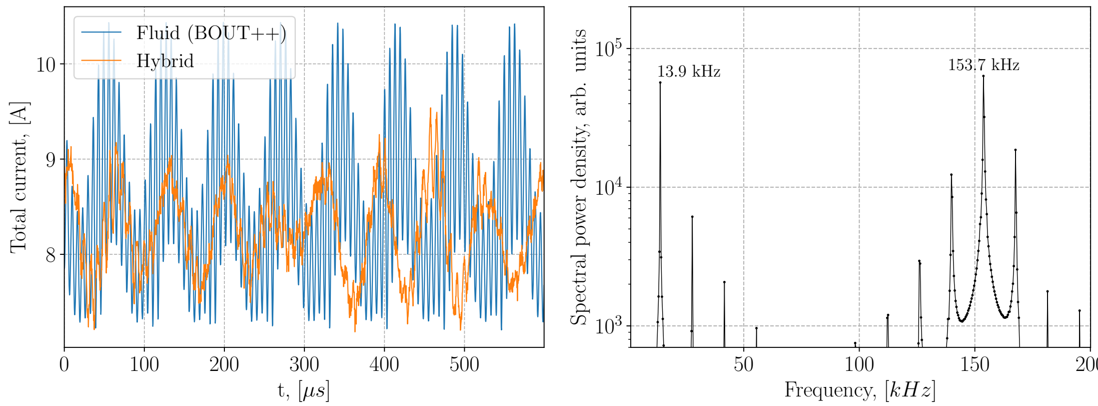

(a) (b)

Figure 5. Comparison of total current in the fluid model and hybrid model, when ion pressure term is included into fluid model with constant temperature $T_i = 1.2\ eV$ (a), Case 1.

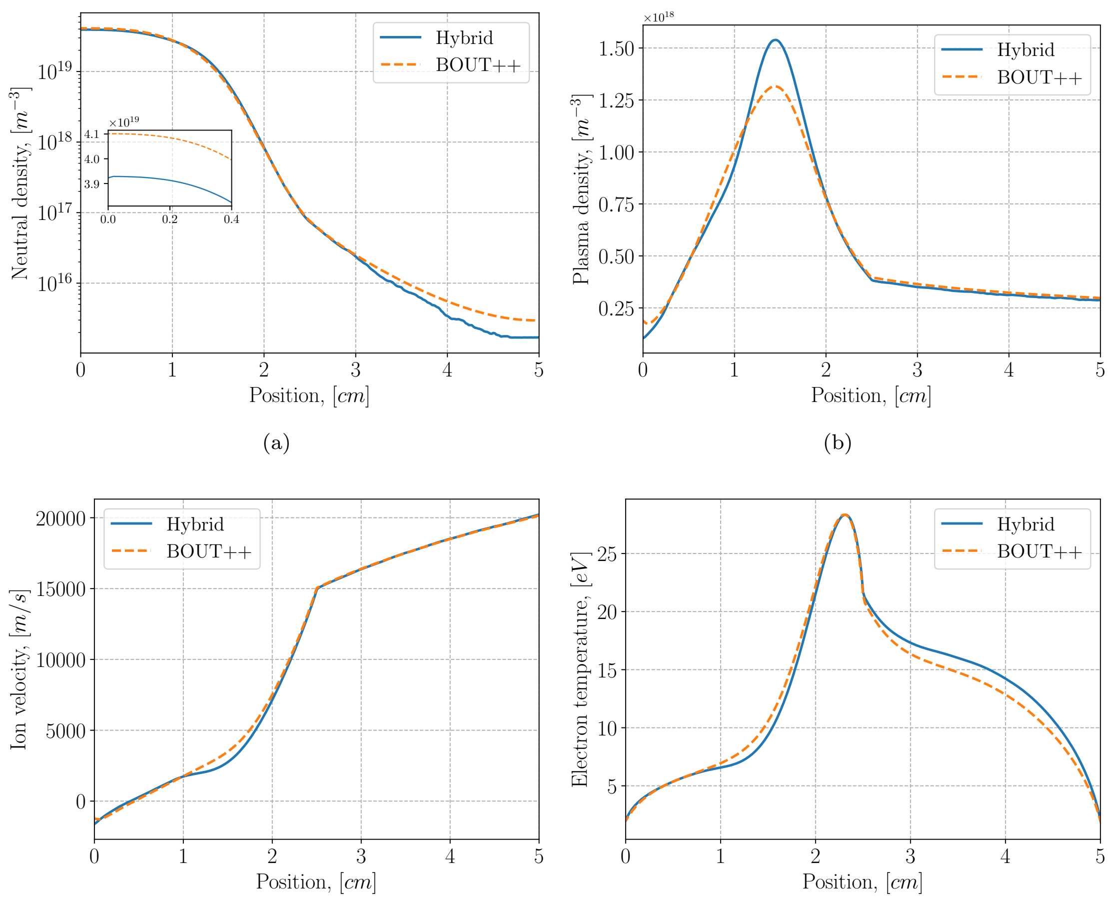

(a) (b)

(c) (d)

Figure 6. Comparison of spatial distribution of time averaged macroscopic profiles between fluid and hybrid models, when ion pressure term is included into fluid model with constant temperature $T_i = 1.2\ eV$, Case 1.

B. Case 2

This case is subject to low-frequency oscillations only. As in the previous case, the fluid model results in the higher total current amplitude, Figs. 7a, 7b, but the main frequency component in the spectral density is about the same, Figs. 8a, 8b.

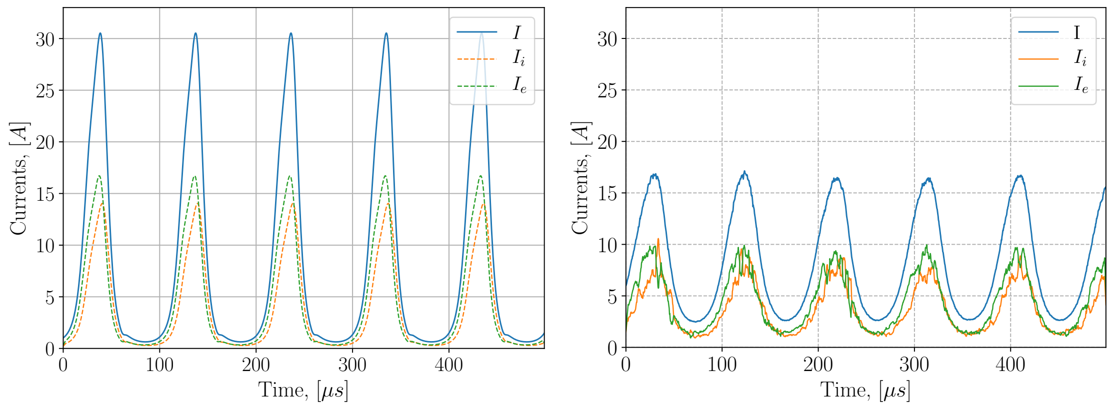

Figure 7. Total, ion, and electron current result from fluid model (a) and hybrid model (b). Ion and electron currents are evaluated at $x = 5$ cm, Case 2.

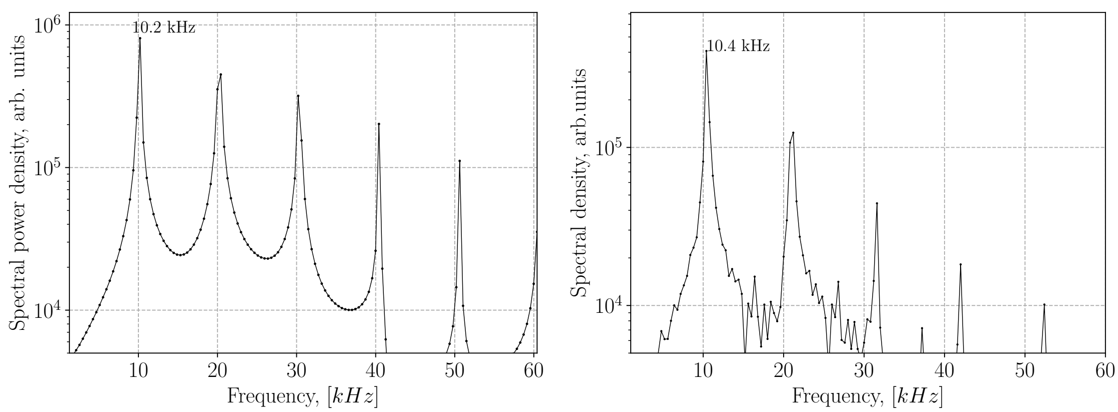

Figure 8. Spectral density of the total current for fluid model (a) and hybrid model (b), Case 2.

Time averaged profiles are mostly close to each other, and only plasma density in the fluid model is $\sim 30\%$ lower inside the channels region, Figs. 9a-9d.

It is noted that in this case the ion temperature from the hybrid model is low enough, Fig. **??**, thus it will not affect the results notably. But the oscillation dynamics in this case clearly shows that the plasma recombination at the anode (21) is deeply involved into the low-frequency behaviour. Turning off the recombination mechanism nullifies the oscillations and results into a stationary solution, in both models. The illustration of the oscillation dynamics is presented in Fig. 10. Here the main stages of this low-frequency dynamics presented with plasma and atom densities. After atoms reach the ionization zone and undergo ionization, plasma density increases and quickly expelled to the left (due to the backflow region with negative velocity) and the right of ionization zone. Then all of the ion flux that reached the anode recombines (21) and form the peak in neutral density at the anode, and increased number of atoms is moved to the ionization zone and this process repeats.

It is clearly seen that the oscillations in this case has to do with the backflow region, which transfers some part of the plasma to the left, it recombines into atoms and returns back to the ionization zone. The average position of zero ion velocity here is ~ 1.1 cm, and the time required for atoms to reach this point is

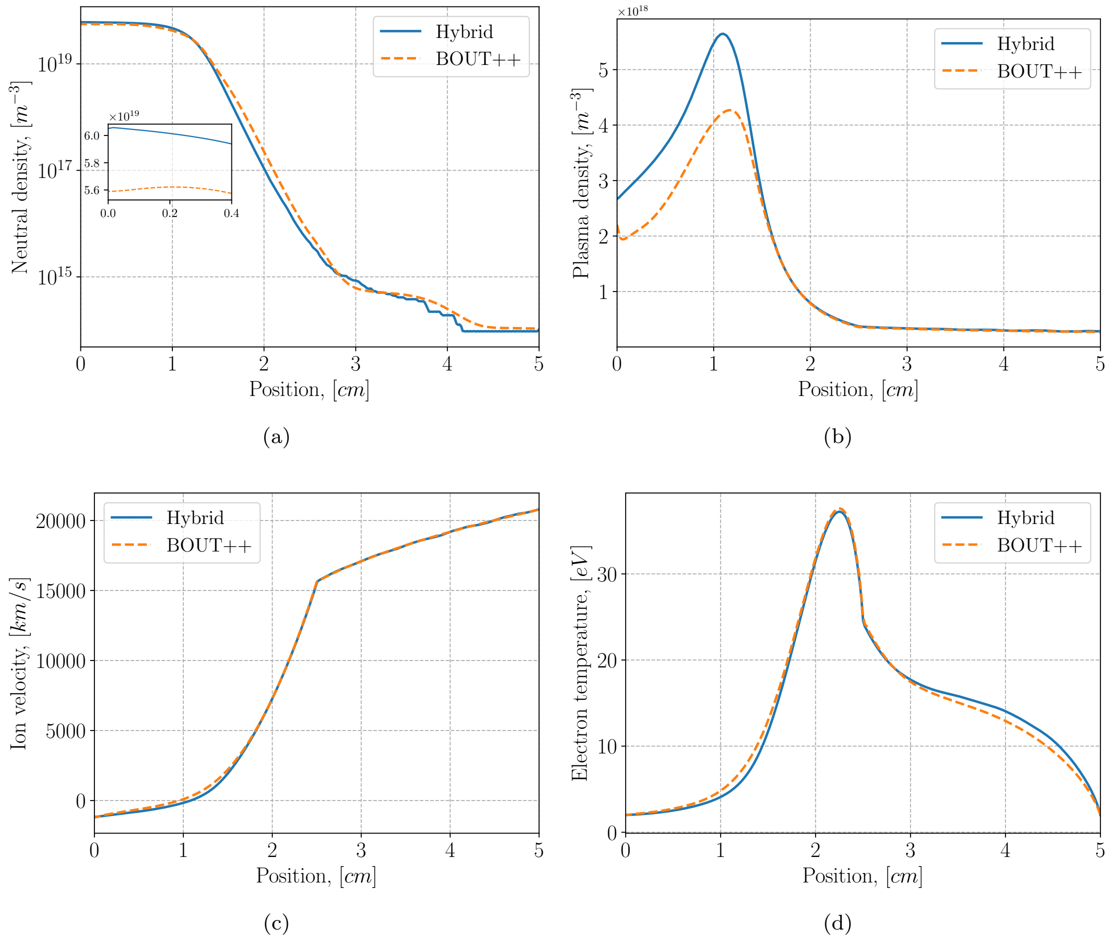

Figure 9. Comparison of spatial distribution of time averaged macroscopic profiles between fluid and hybrid models, Case 2.

$\sim 73\ \mu s$. We should add the time of ionization process itself, $t \approx (N_2 - N_1)/S \approx 20\ \mu s$, where N_2 and N_1 are atom densities in the beginning and end of ionization process, respectively, and S is an average source term in this region. Finally, with the time for plasma backflow to the anode is $m11\mu s$, it comes close to observed value of oscillation period of $m100\ \mu s$, Fig. 7a. This is supported with about linear scale is observed between neutral flow velocity and resulted frequency, Fig. 11b.

We suggest that the main difference in this case between the fluid and the hybrid model is in ion velocity boundary condition. Normally, in the fluid quasineutral models this boundary condition is fixed to the Bohm velocity. As noted before, the recombination of plasma at the anode strongly affects oscillations in this case, thus difference in boundary conditions can potentially explain the observed discrepancy. When Bohm boundary condition is decreased in the fluid model, the oscillations amplitude is also decreases, see Fig. 11a. It can be explained as decreased ion velocity decreases the amount of recombined plasma and it decreases overall oscillations amplitude. But in the present hybrid model ions are not forced to satisfy Bohm condition, it oscillates in time, Fig. 12a. We modeled this behaviour with the free boundary condition for ion velocity at the anode in the fluid model, forcing $\partial_x^2 v_i(0) = 0$. It results in a less violent oscillations and a better agreement with the hybrid model. The total current amplitude is lower, Fig. 13a and its spectral components, Fig. 13b better agree with the hybrid result. Neutral and plasma densities agreement is improved, Figs. 14a, 14b.

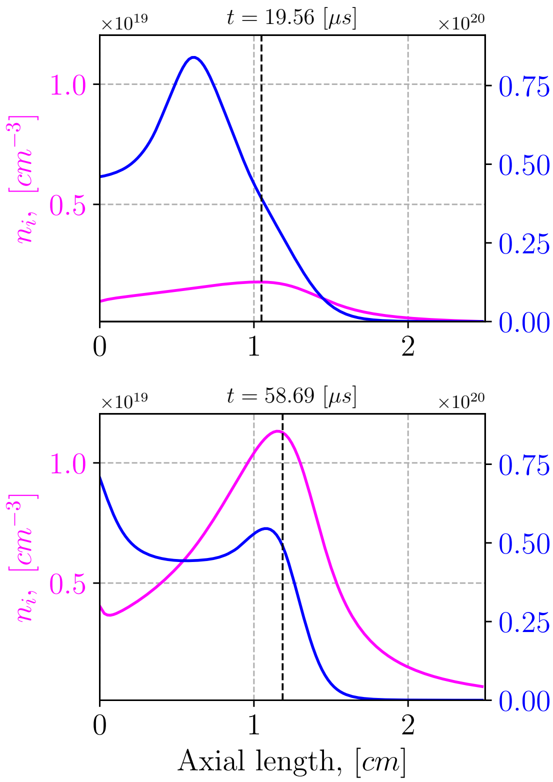

Figure 10. Neutral and plasma density evolution during one oscillation period. Dashed line separates the region with negative (to the left) and positive (to the right) ion velocity.

C. Case 3

In this case the hybrid model allowed for a finite atoms temperature, initializing them with $T_a = 500\ K$. At the anode, new neutral particles are injected with the same temperature. As a result, no more low-frequency oscillations were observed. The main difference with previous case has to do with neutral dynamics. In fact, we noted that average neutral velocity changes significantly along the channel (accelerating). This effect is known selective ionization, observed both in experiments[18,19] and hybrid simulations.[6] Atoms are "accelerating" due to the fact that slower particles are more probable to ionize when passing through the ionization region, as they spend longer time there. The most obvious solution of this issue in the fluid model is including the atoms momentum balance equation,

$$\frac{\partial (n_a v_a)}{\partial t} + \frac{\partial}{\partial x}\left(n_a v_a^2\right) = -\beta n_a n_i v_a - \frac{1}{m_i}\frac{\partial (n_a T_a)}{\partial x}, \tag{22}$$

which can be written in non-conservating form (substituting atom continuity Eq.1) as

$$\frac{\partial v_a}{\partial t} + v_a \frac{\partial n_a}{\partial x} = -\frac{1}{m_i}\frac{\partial (n_a T_a)}{\partial x}. \tag{23}$$

The validity of this equation is confirmed by calculations of fluid moments from kinetic part of the hybrid model, and thus checking that the atom momentum balance equation in this form is complete. Again, we assumed that the pressure tensor is isotropic, and so the atom temperature is evaluated as $T_{ax} = p_{a,xx}/n_a$, where $p_{a,xx} = m_i \int v_x' v_x' f_x dv_x$, where $v_x' = v_x - V_x$ is the random particle velocity.

In the hybrid model atoms are initialized with 500 K temperature, or the thermal velocity $v_{Ta} = 252\ m/s$, which corresponds to the axial thermal velocity part $v_{Tax} = 145\ m/s$ (isotopic velocity distribution). The value v_{Tax} is set as the fixed boundary condition at the anode, and constant $T_a \sim 167K$ is assumed in the fluid calculations. As a result, the fluid model produces a fully stationary solution with the total current of 8.0 A, and in the hybrid model the average total current is 7.9 A, Fig. 15.

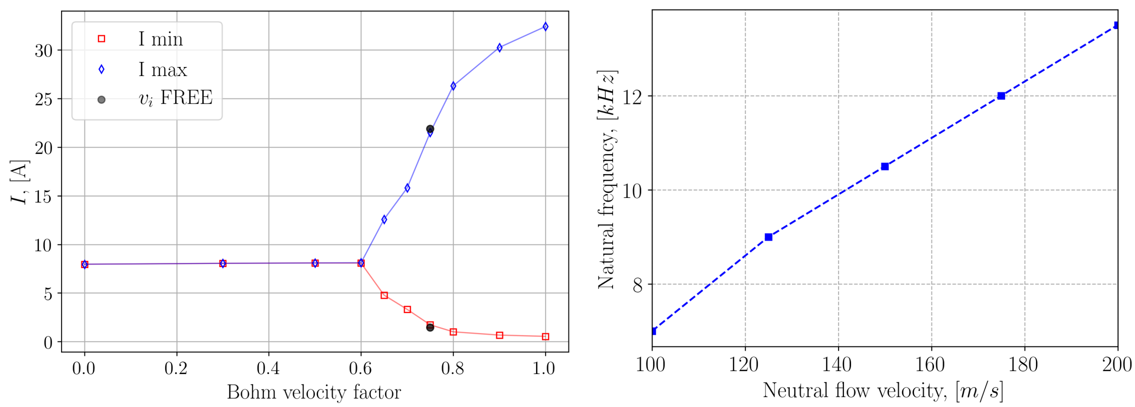

(a) (b)

Figure 11. Minimum and maximum total current values during oscillations for various ion velocities at the anode, expressed as fractions of the Bohm velocity (a). Note that oscillations are absent for $v_i < -0.6C_s$. Natural frequency of low-frequency oscillations as a function of constant neutral atom flow velocity (b).

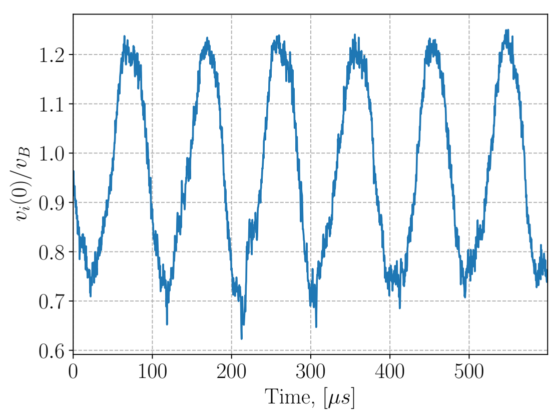

Figure 12. Average ion velocity at the anode in hybrid model.

Interestingly, we were not able not find low-frequency oscillations by changing parameters ν_ε or β_a when atom velocity distribution is included.

IV. Summary

Low-frequency axial simulations of a Hall thruster are performed in the fluid and the hybrid (kinetic/fluid) models, and comparison between the results is presented. It is shown that in general results are qualitatively similar with some quantitative differences when atoms are monoenergetic (zero temperature, same "average" velocity). In these cases we were able to improve the agreement by either accounting for ion pressure term (with constant temperature) in the ion momentum balance equation (3) or by modifying ion velocity boundary condition (replacing fixed Bohm to a free boundary condition at the anode). In the case with finite atom temperature in the hybrid model it is shown that the advection equation with constant flow velocity is not sufficient to describe atom dynamics in the fluid model. A strong effect of selective ionization of neutral particles is observed in this case, where average macroscopic velocity increased more than twice along the channel. To account for this effect, the fluid model had to be solved with the neutral atoms momentum balance equation (23), which resulted in a good agreement between two models.

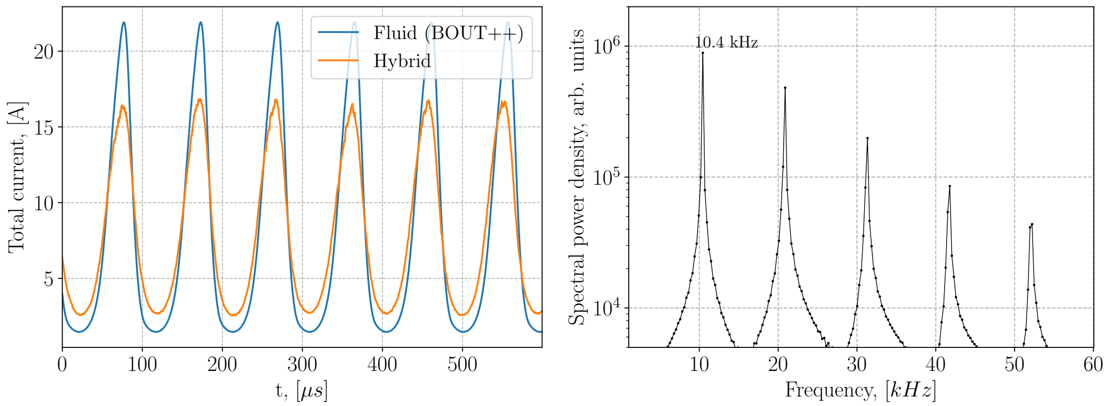

Figure 13. Total current comparison and spectral power density for total current in fluid model, Case 2.

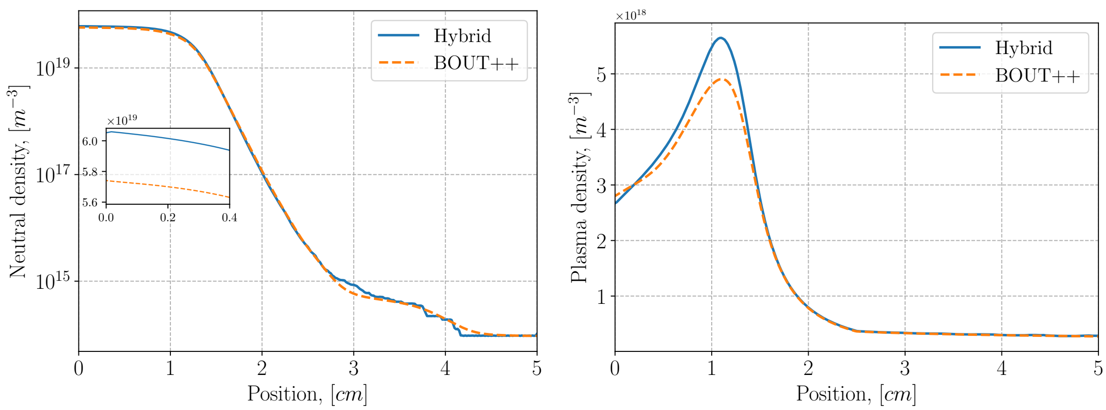

(a) (b)

Figure 14. Comparison of spatial distribution of time averaged macroscopic profiles between fluid and hybrid models, Case 2.

Acknowledgments

This work is supported in part by NSERC Canada, and US Air Force Office of Scientific Research FA9550-15-1-0226.

References

[1]AI Morozov and VV Savelyev. Fundamentals of stationary plasma thruster theory. In *Reviews of plasma physics*, pages 203–391. Springer, 2000.

[2]GJM Hagelaar, J Bareilles, LBJP Garrigues, and J-P Boeuf. Two-dimensional model of a stationary plasma thruster. *Journal of Applied Physics*, 91(9):5592–5598, 2002.

[3]S. Barral and E. Ahedo. Low-frequency model of breathing oscillations in hall discharges. *Physical Review E*, 79(4):046401, 2009.

[4]JP Boeuf and L Garrigues. Low frequency oscillations in a stationary plasma thruster. *Journal of Applied Physics*, 84(7):3541–3554, 1998.

[5]S Chable and F Rogier. Numerical investigation and modeling of stationary plasma thruster low frequency oscillations. *Physics of plasmas*, 12(3):033504, 2005.

[6]K Hara, ID. Boyd, and VI Kolobov. One-dimensional hybrid-direct kinetic simulation of the discharge plasma in a hall thruster. *Physics of Plasmas*, 19(11):113508, 2012.

[7]E Ahedo, P Martınez-Cerezo, and M Martınez-Sánchez. One-dimensional model of the plasma flow in a hall thruster. *Physics of Plasmas*, 8(6):3058–3068, 2001.

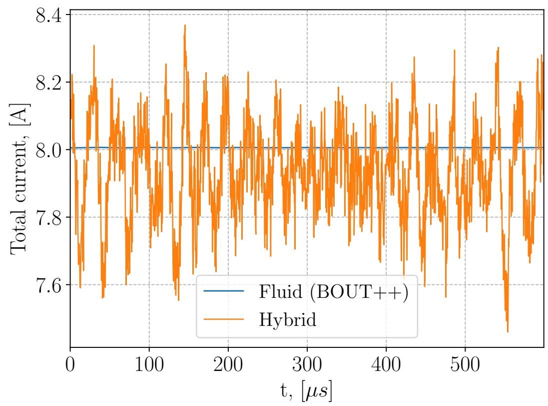

(a)

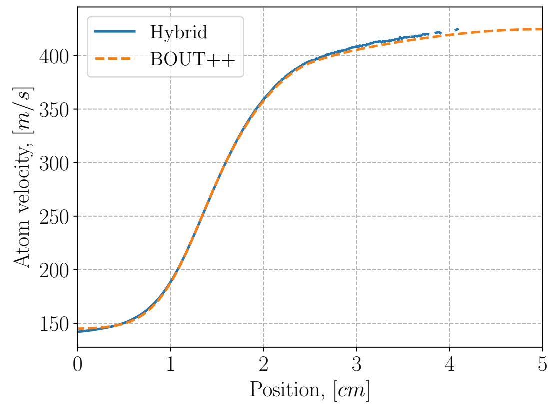

(b)

Figure 15. Fluid and hybrid models comparison of total current (a) and averaged in time spatial profile of atom velocity (b), Case 3.

[8]A Fruchtman, NJ Fisch, and Y Raitses. Control of the electric-field profile in the hall thruster. *Physics of Plasmas*, 8(3):1048–1056, 2001.

[9]A Cohen-Zur, A Fruchtman, and JGA Ashkenazy. Analysis of the steady-state axial flow in the hall thruster. *Physics of Plasmas*, 9(10):4363–4374, 2002.

[10]E Ahedo, JM Gallardo, and M Martınez-Sánchez. Model of the plasma discharge in a hall thruster with heat conduction. *Physics of Plasmas*, 9(9):4061–4070, 2002.

[11]Low temperAture magNetizeD plasMA benchmaRKs. `https://www.landmark-plasma.com/`.

[12]S Barral, Z Peradzynski, K Makowski, and Michel A Dudeck. Fluid model of hall thruster-comparison with hybrid model. *High Temperature Material Processes: An International Quarterly of High-Technology Plasma Processes*, 5(2), 2001.

[13]BD Dudson, MV Umansky, XQ Xu, PB Snyder, and HR Wilson. Bout++: A framework for parallel plasma fluid simulations. *Computer Physics Communications*, 180(9):1467–1480, 2009.

[14]GJM Hagelaar, J Bareilles, L Garrigues, and J-P Boeuf. Role of anomalous electron transport in a stationary plasma thruster simulation. *Journal of Applied Physics*, 93(1):67–75, 2003.

[15]GJM Hagelaar, J Bareilles, L Garrigues, and J-P Boeuf. Modelling of stationary plasma thrusters. *Contributions to Plasma Physics*, 44(5-6):529–535, 2004.

[16]GJM Hagelaar and LC Pitchford. Solving the boltzmann equation to obtain electron transport coefficients and rate coefficients for fluid models. *Plasma Sources Science and Technology*, 14(4):722, 2005.

[17]EY Choueiri. Plasma oscillations in hall thrusters. *Physics of Plasmas*, 8(4):1411–1426, 2001.

[18]NB Meezan, WA Hargus Jr, and MA Cappelli. Anomalous electron mobility in a coaxial hall discharge plasma. *Physical Review E*, 63(2):026410, 2001.

[19]WA Hargus and MA Cappelli. Interior and exterior laser-induced fluorescence and plasma measurements within a hall thruster. *Journal of Propulsion and Power*, 18(1):159–168, 2002.

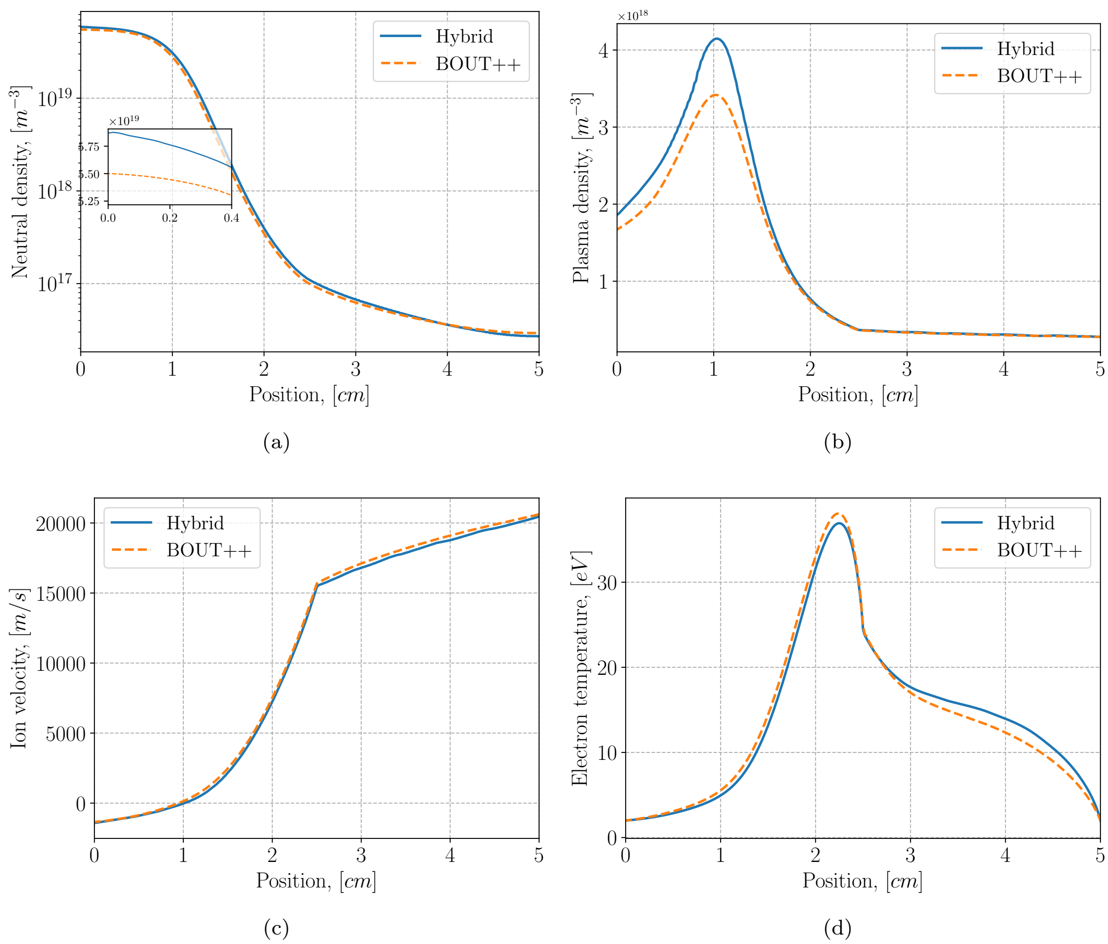

Figure 16. Comparison of spatial distribution of time averaged macroscopic profiles between fluid and hybrid models, Case 3.